# Molecule-Graphene Hybrid Materials with Tunable Mechanoresponse: Highly Sensitive Pressure Sensors for Health Monitoring

Paolo Samorì, Chang-Bo Huang, Alessandro Aliprandi, Marc-Antoine Stoeckel, Massimo Bonini, Artur Ciesielski, Samanta A Witomska

DOI: 10.1002/((please add manuscript number))
**Article type: Communication**

# Molecule-graphene hybrid materials with tunable mechanoresponse: highly-sensitive pressure sensors for health monitoring

*Chang-Bo Huang,[1] Samanta Witomska,[1,2], Alessandro Aliprandi,[1] Marc-Antoine Stoeckel,[1] Massimo Bonini,[3] Artur Ciesielski,[1,*] and Paolo Samorì[1,*]*

[1] C.-B. Huang, S. Witomska, Dr. A. Aliprandi, M.-A. Stoeckel, Dr. A. Ciesielski, Prof. P. Samorì
University of Strasbourg, CNRS, ISIS UMR 7006, 8 Alleé Gaspard Monge, F-67000 Strasbourg, France.
E-mail: ciesielski@unistra.fr , samori@unistra.fr

[2] S. Witomska
Faculty of Chemistry and Center for Advanced Technologies Adam Mickiewicz University, Umultowska 89b/89c, 61614 Poznań, Poland.

[3] Prof. M. Bonini
Department of Chemistry "Ugo Schiff" and CSGI, University of Florence, via della Lastruccia 3, Sesto Fiorentino, 50019 Florence, Italy.

Keywords: Functionalized graphene, molecular self-assembly, pressure sensor, tunable mechanoresponse, health monitoring

Pressure sensors are devices capable of generating electrical signals in response to a change in pressure.[1-2] Such devices hold great technological potential as they can become key elements for wearable bioelectronics applications,[3-5] e.g. by monitoring the wearers' health[6-9] and their surroundings.[10-12] Numerous electroactive materials have been exploited as active components including graphene,[10, 13-16] carbon nanotubes (CNTs),[5, 17] conductive elastomers,[4, 18] silicon nanowires and nanostrips,[19] metal nanowires and nanoparticles.[20] Among them, graphene has been the most studied due to its excellent electrical conductivity,[21] high transmittance,[22] outstanding mechanical properties[23] and large surface area.[24-25] Noteworthy, graphene can be safely employed in devices being in direct contact with human skin, enabling applications as tattoo sensors.[26]

To evaluate the performance of pressure sensor, several parameters need to be taken into account such as sensitivity, response time, detection limit, linearity range, cyclability, power

consumption and robustness. The sensitivity of the pressure sensor, defined as the ratio between the change in the electrical signal output and the applied pressure, is probably the most important figure-of-merit of the sensor. Sensors featuring high sensitivities are capable of detecting extremely small changes in the pressure, and can be exploited even to transduce muscle movements[16, 27] as well as the subtle vibrations of sound[6, 11, 28-29] into electrical outputs. Compared to the complicated fabrication methods such as microelectromechanical systems (MEMS)[30-31] and microfluidics techniques[7], the engineering of the structure of active material represents the simplest and the most straightforward approach for the fabrication of pressure sensors in which a small applied pressure can determine subtle structural changes in the electroactive material. For example, upon applying a pressure, cracks and structural defects can be generated, which results in modification of the percolation pathways for charge transport, and can ultimately result in large variations in the electrical output.[13, 32-33] Moreover, the contact resistance at the electrode-active layer interface can be modulated by pressure resulting into an improvement of the sensitivity.[12, 18, 34-35] By using such a strategy, Suh *et al.*[35] demonstrated a strain-gauge sensor, which is based on two interlocked arrays of Pt-coated polyurethane acrylate nanofibres supported on thin polydimethylsiloxane layers. Furthermore, a change in capacitance can be induced by pressure, which is the working principle of capacitive pressure sensor. In that case the sensitivity can be improved by micro structuration of the dielectric layer between electrodes.[8, 36-37] Bao *et al*.[37] reported a field-effect transistor (FET) based pressure sensor which employed a microstructured pyramid-like polydimethylsiloxane (PDMS) film as dielectric layer. The sensitivity has been effectively increased to 0.55 $kPa^{-1}$, which is much higher than that of the unstructured one. Although these methods can indeed improve the sensitivity of the device, their applications are generally limited due to the complicated nature of the fabrication process, high production cost and high operating voltage. Conversely, piezoelectric sensors are usually not chosen because they display lower pressure sensitivities and can be hardly integrated into flexible electronic skins.[37]

Here, we have developed a novel simple method to drastically improve the sensitivity of a piezoresistive pressure sensor. The active material has been assembled by reacting commercially available graphene oxide (GO) with amino functionalized molecules in order to form covalent bonds on the basal plane of GO through the epoxy ring-opening reaction (Figure 1a). Three organic molecules characterized by a similar contour length and increasing rigidity, namely triethylene glycol (TEG) amine (**R1**), 1-octylamine (**R2**) and 4-aminobiphenyl (**R3**) were chosen as the molecular units. Upon condensation of **R1**-**R3** with GO, hybrid structures are obtained in the form of ink dispersed in ethanol. In this way the growth of molecular pillars occurs specifically along the axis perpendicular to the graphene basal plane,[38] yet, the amidation of carboxyl groups, present at the edges of GO sheets may occur as a side reaction. Such chemically modified GO (CMGO) has been chemically reduced with hydrazine[39] to restore high electrical conductivities (for details see Supporting Information). The as-obtained conducting ink can be deposited onto arbitrary substrates by spray-coating, yielding multilayer structures with spacing between adjacent GO sheets which are dictated by the employed molecular pillars, i.e. **R1**-**R3** molecules. Significantly, the latter possess different compressibility, resulting from the intrinsic flexibility of the chosen molecules. The CMGO containing molecules possessing the highest flexibility should display the largest compressibility at a given pressure, thus leading to the highest sensitivity to detect changes of pressure. In analogy to the Hooke's law ruling the compressibility of macroscopic springs, we demonstrate that the sensitivity of the pressure sensor can be improved from **rGO-R$_3$** (0.32 kPa$^{-1}$) to **rGO-R$_1$** (0.82 kPa$^{-1}$) by using more flexible linkers acting as molecular springs separating rGO layers (Figure 1b). Compared to the other approaches employed so far,[13, 35, 37] this method shows several additional advantages that render it of potential interest for technological applications including the low cost production, simple device fabrication and low operating voltage (0.2 V).

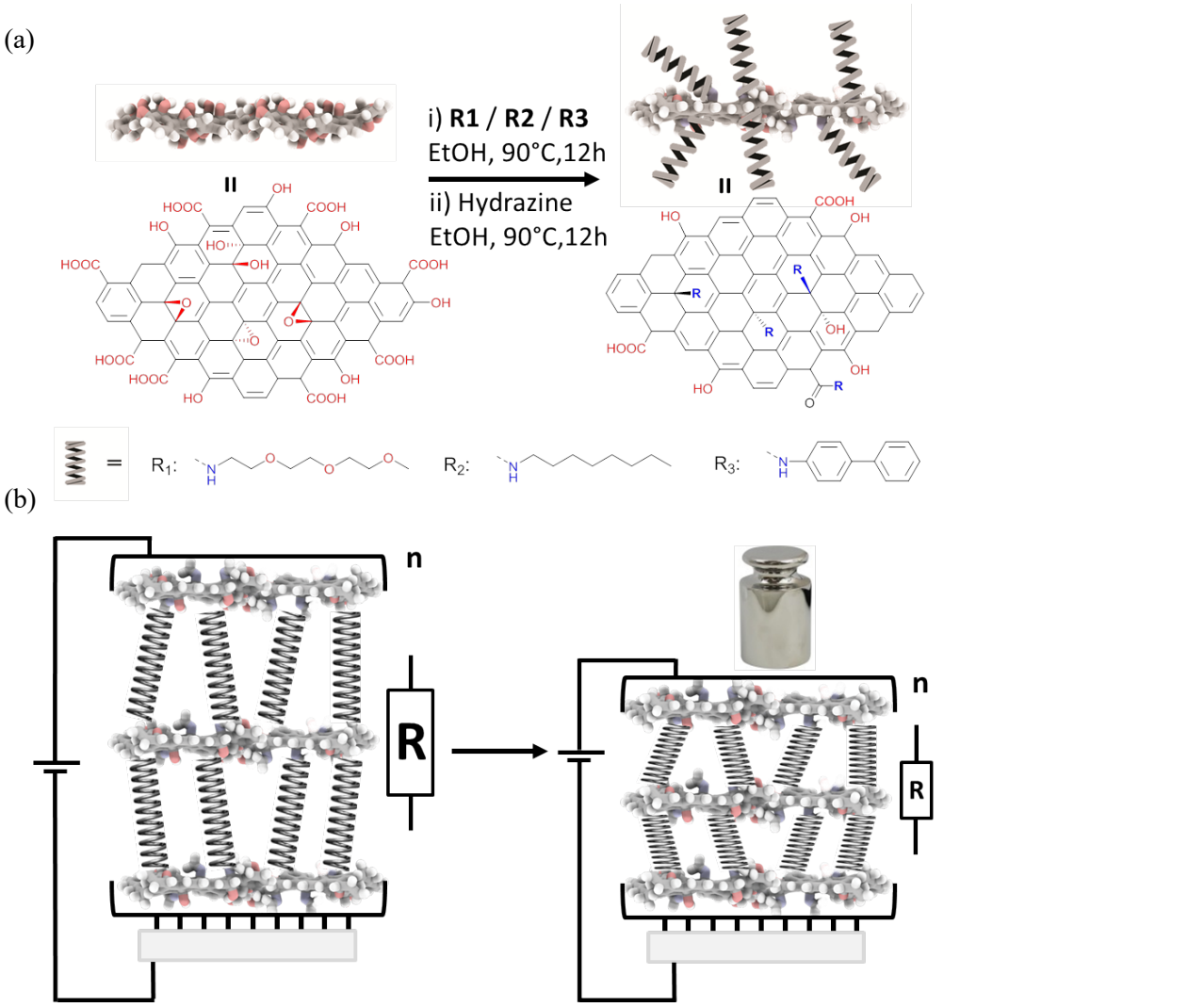


**Figure 1.** (a) Synthesis and architecture of **rGO-R$_1$**, **rGO-R$_2$**, and **rGO-R$_3$**. (b) Schematic of working principle of the pressure sensor.

The multiscale characterization of various physico-chemical properties of the GO based hybrid structures have been carried out using different experimental techniques. X-ray photoelectron spectroscopy (XPS) provided quantitative insight into the chemical composition of hybrid material. In particular, the significant difference between the carbon, oxygen and nitrogen peaks provided evidence for the formation of a chemical bond between the oxygen-containing functional groups on the surface of GO and amine groups from **R1**-**R3** molecules (Figure S2, S3, and S4). The interlayer distance ($d_{002}$) between modified GO sheets with **R** molecules is characterized by wide-angle X-ray scattering (WAXS). After functionalization

the 2θ peak of **GO-R$_{1-3}$** shifts toward lower angles compared to pristine GO, which indicates an increase in the interlayer distance (Figure S5). The efficiency of the reaction has also been confirmed by Raman spectroscopy (Figure S6) and infrared spectroscopy (FTIR) (Figure S7). The porosity of functionalized graphene has been investigated by the means of BET measurements (Figure S8). Details on the details of analysis and results there of obtained by XPS, WAXS, Raman, BET and FTIR are provided in the Supporting Information.

The pressure sensors have been fabricated by following the procedure displayed in Figure 2a. Functionalized reduced graphene oxide inks (**rGO-R$_1$**, **rGO-R$_2$** or **rGO-R$_3$**) have been spray-coated through a shadow mask onto the surface of ITO-PET. The amount of deposited material was monitored by UV-Vis absorption as shown in Figure S10. Images of scanning electron microscopy (SEM, Figure S11) display flakes stacked perpendicularly to the surface of the electrode forming a multilayer architecture, which can be further verified by the tilted or side view of spray coated **rGO-R$_1$**. After the removal of the shadow mask, two substrates have been fixed together in face-to-face fashion and sealed with Kapton tape preventing the interference of humidity. Finally, the extremities of the PET film have been contacted with copper wires using silver paste.

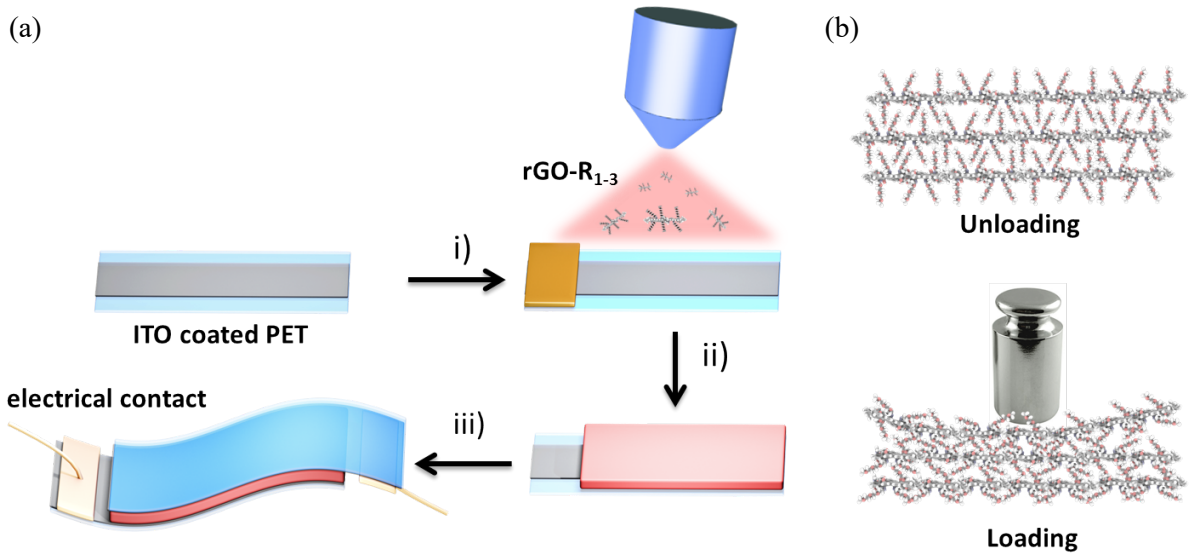

**Figure 2.** (a) Pressure sensor fabrication process: i) spray coating of **rGO-R$_{1-3}$** in presence of a shadow mask on commercially available ITO-PET which was cut into stripes (13 mm × 20 mm); ii) mask removal; iii) face-to-face assembly and wire out with copper wire and silver paste. (b) Schematic illustration of the inner structure change of the functionalized graphene upon loading pressure.

The performance of pressure sensors has been investigated by exploiting a force gauge equipped with a movement-control stand combined with a source-meter to offer a steady bias voltage. Step force from 0.005 N to 1 N has been applied on the device (contact area is 1.04 $cm^2$). The conversion of mechanical displacement into electrical signal is achieved by measuring the current change under different applied forces. The sensitivity of the different pressure sensors can be calculated by using the equation $S=\delta(\Delta R/R_0)/\delta P$, with P being the applied pressure, R and $R_0$ being the resistance with or without applied pressure, respectively.[13] As shown in Figure 3a, the sensitivity of each pressure sensor is defined as $S_1$, $S_2$, $S_3$ and $S_4$ for **rGO-R$_1$**, **rGO-R$_2$**, **rGO-R$_3$** and unfunctionalized rGO (blank experiment) respectively, in the low-pressure region from 0 to ca. 0.6 kPa. Among all the three functionalized graphene based pressure sensors the one containing **R1** pillars, i.e. (**rGO-R$_1$**) shows the highest sensitivity of 0.82 $kPa^{-1}$. The pressure sensor made with **rGO-R$_2$** shows the medium sensitivity of 0.47 $kPa^{-1}$ and the one made with **rGO-R$_3$** shows the lowest sensitivity of 0.32 $kPa^{-1}$. Noteworthy, all the three functionalized graphene based pressure sensors display prominently higher sensitivity than the one based on neat rGO, the latter exhibiting a negligible response (0.073 $kPa^{-1}$).

The detected difference in sensitivities can be explained by the fact that the current passing through the rGO-based vertical junction is strongly affected by extremely small changes of the interlayer distance between the rGO sheets, which is in turn dictated by the flexibility (or conformation) of the molecular bridges (Figure 2b). Laser Scanning Confocal Microscopy

(LSCM) measurements revealed that the interlayer distance of functionalized graphene materials decreases when a pressure is applied (Figure S9), thus yielding an increase in the tunnelling current. The contribution to resistance variation determined by the contact resistance has been found being negligible as revealed by performing blank experiment with neat rGO as active material (Figure 3a, green line) and the effect caused by pore structure has been excluded by BET analysis (Table S1, Figure S8). The electron transport mechanism has been proved to be direct electron tunnelling by temperature dependent electrical conductivity measurement (see Figure S12 in for detail analysis). The molecular flexibility is related to the intrinsic conformational degree of freedom of carbon and/or oxygen atoms around their chain bonds. Persistence length ($L_p$) has been widely used to quantify the flexibility or stiffness of polymers, in which the smaller is the $L_p$, the more flexible is the polymer.[40-42] Here the three molecular linkers **R1**, **R2** and **R3** can be considered as small oligomers of polyethylene glycol (PEG), polyethylene (PE) and poly-(p-phenylene) (PPP) polymers, respectively. Thus, by considering the $L_p$ of each polymer, which amounts to 0.37 nm for PEG[40], 0.65 nm for PE[41] and 28 nm for PPP[42], **R1** should be the most flexible linker while **R3** the most rigid one. The trend we have observed for the sensitivity is in excellent agreement with the different $L_n$ of the molecular linkers suggesting that the more flexible is the linker the higher is the sensitivity. Furthermore, the vertical amplitude of the error bar associated to $\Delta R/R_0$ (Figure 3a) is increasing as $L_n$ is decreasing, suggesting that flexible linkers can possess different conformations at the same pressure.

The response of the devices to a dynamic force has also been investigated through finger press, bending test, light object trigger and fatigue test. For these experiments, the pressure sensor containing **rGO-R$_1$** as active material has been employed due to its highest sensitivity. As shown in Figure 3b, quick press and release of a finger on the device leads to a quick response, which results in sharp peaks of current. The response time ($t_1$) and recovery time ($t_2$) of **rGO-R$_1$** are 24 ms and 10 ms (inset in Figure 3b) respectively, which are 3~5 times faster

than those reported for pressure sensors made with reduced graphene oxide.[10, 43] Figure 3c shows the dynamic response of pressure sensor **rGO-R$_1$** during bending test. During bending cycles (1.5 cm bending radius, 100° degree bending angle) sharp peaks of current have been recorded demonstrating high flexibility and robustness of the sensor. By taking full advantage of the high sensitivity, the pressure sensor can also detect ultra-small pressure fluctuations as tiny as 7 Pa. A paper-folding star (ca. 70 mg, corresponding to 7 Pa, inset in Figure 3d) has been placed-and-removed continuously onto the pressure sensor, causing a distinct change of current. The ability of sensing such small pressures once again represents an unambiguous evidence of the high sensitivity of this material and device thereof. The excellent cyclability of the device has been verified by fatigue test as shown in Figure S13. After 2000 cycles of press-release with the pressure of 3 kPa, the on-state signal is still stable, demonstrating the high robustness of the device which is fundamental for a future commercialization. The negligible upper shift of baseline might be caused by some irreversible deformation of graphene layers between flexible electrodes.

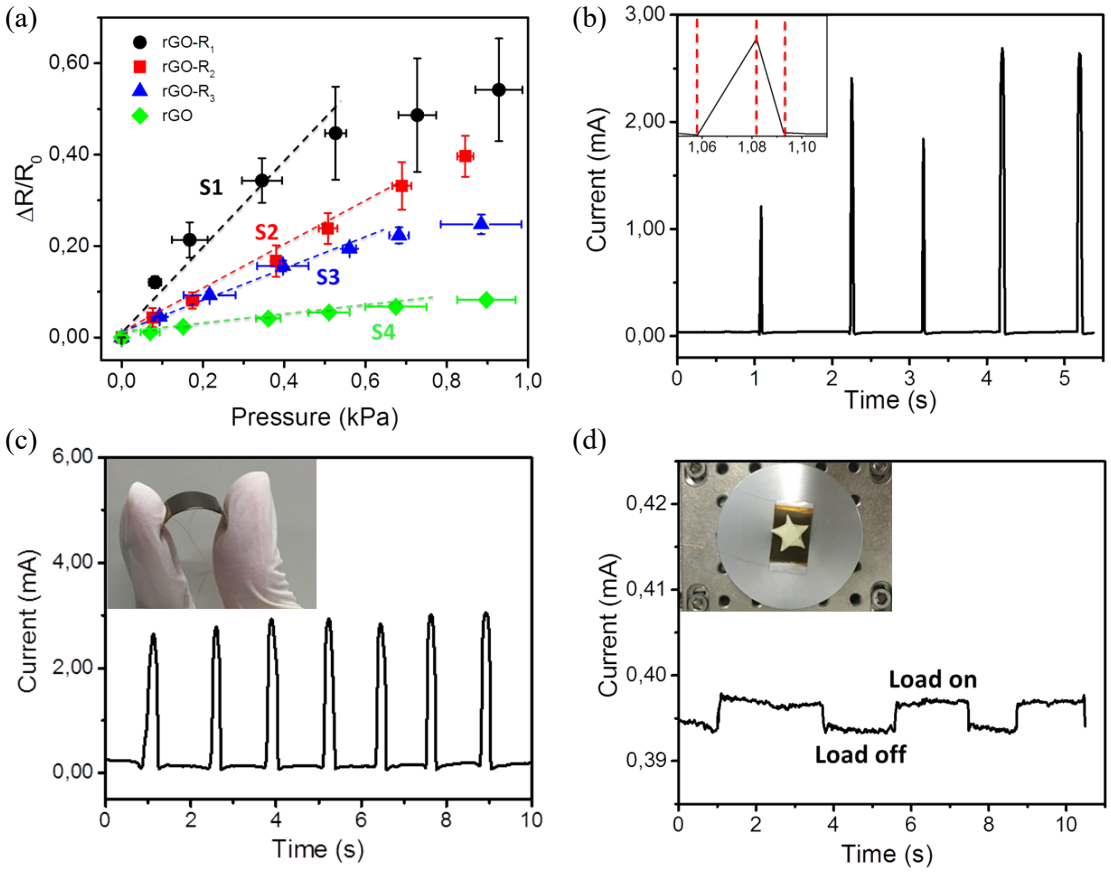


**Figure 3.** (a) Relative resistance as a function of the pressure applied for sensor **rGO-R$_1$** (black circles), **rGO-R$_2$** (red squares), **rGO-R$_3$** (blue triangle), and rGO (green diamond) (error bar: mean±SD). Response of pressure sensor **rGO-R$_1$** to consecutive finger press (b), bending test (c) and light object (d) (inset: a paper folding star, ca. 70 mg, corresponding to the pressure of 7 Pa).

Due to the high sensitivity, fast response to both pressure changes and bending as well as ultralow detection limit and high robustness, such pressure sensor can be implemented into wearable electronic devices for healthcare, human-machine interface, and digital tactile system etc. As a proof-of-concept we have employed the pressure sensor (**rGO-R$_1$**) to monitor wrist pulse and carotid artery pulse of an adult male, which are generally used to evaluate the health condition of human body.[8, 44] As shown in Figure 4a, the pressure sensor has been placed on an adhesive bandage and fixed to the wrist or to the neck of the human

subject. A stationary signal has been recorded from which the radial artery frequency (65 pulses $min^{-1}$) and carotid artery frequency (61 pulses $min^{-1}$) can be obtained, indicating that the subject in good health condition as an adult male. More importantly, due to the high resolution of the radial artery pulse curve, we can clearly observe two distinguish peaks, P1 which refers to the sum of ejected wave and reflected wave, and P2 which is the peak of the reflected wave from the lower body minus end-diastolic pressure. Thus we can calculate two important parameters, i.e. the radial artery augmentation index ($AI_r$) and the time between two peaks ($\Delta T_{DVP}$), which are commonly used for arterial stiffness diagnosis.[44] According to the measured results, $AI_r \approx 61\%$, $\Delta T_{DVP} \approx 0.26$ s further verify the good health condition of the subject. All these results indicate that the pressure sensor (**rGO-R$_1$**) can be successfully applied to human health monitoring.

Furthermore, we provide a demonstration of a sensor matrix by assembling the PET-ITO thin strips to a network as shown in Figure S14. In this way the sensor can be used not only to measure the pressure, but to capture spatial information. Each cross point will indeed act as a pressure sensor and used as pixel to form a rough 3D mapping. The sensing matrix is made with a similar architecture of the pressure sensors discussed above, which is composed by ITO-PET as electrodes and **rGO-R$_1$** as active material in between. The pressure is determined by measuring the change of relative resistance ($\Delta R/R_0$) of each pixel. As shown in Figure 4d, a bolt (mass = 6.1 g) with an annular bottom was placed on the matrix and its contact area (white dash circle) corresponds to the pixels plotted by the electrical output. The highest relative resistance change ($\Delta R/R_0$) occurs in pixel “3D”, which indicates the center of gravity of the bolt. This pressure sensor matrix is also applicable for objects with irregular contact area. Figure 4e reveals the four contact points of a stone (mass = 67.2 g), whose weight is mostly located in position “4C”. By expressing the pressure value in the Z-scale of each pixel, a 3D map of the weight distribution has been obtained as shown in Figure 4f. Such results

provide clear evidence for the potential of such arrays for being implemented into multi-touch devices.

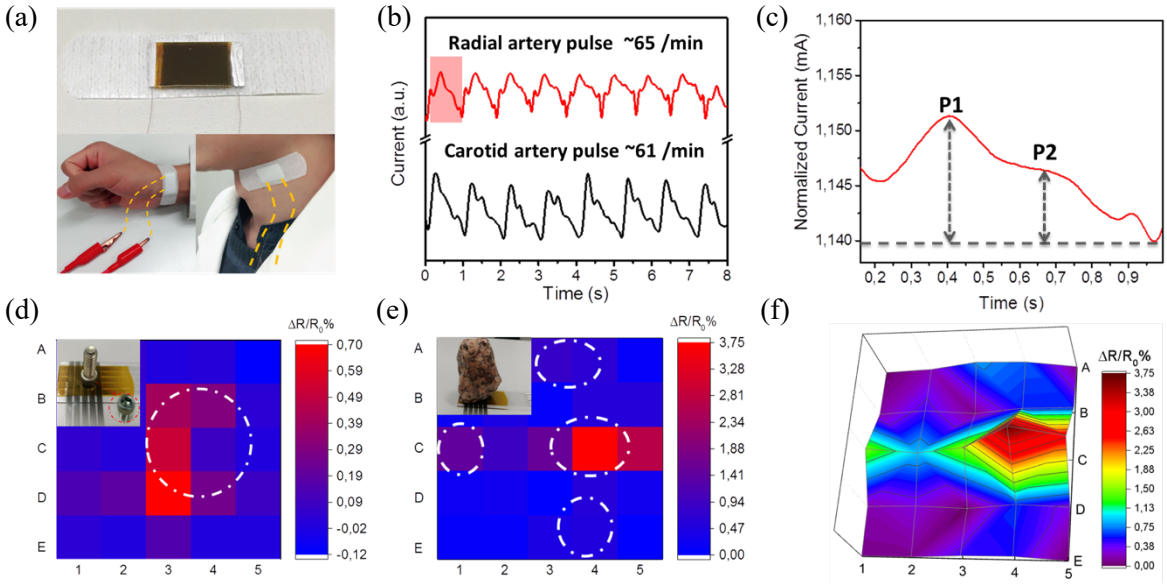


**Figure 4.** Sensing application on human health monitoring (a-c) and sensor matrix for 3D mapping (d-f). (a) radial artery pulse and carotid artery pulse detection assembled by adhesive bandage; (b) The signals of radial artery pulse (top) and carotid artery pulse (bottom). (c) Magnification of a single peak of radial artery pulse (marked with a red square in Figure 4b). Relative resistance mapping of pressure sensor matrix when putting a bolt (d) or a stone (e) on the pressure sensor matrix (white circles: actual contact area). (f) 3D map of the pressure distribution of the stone in Figure 4e.

In summary, we have described a novel method to tune and boost the sensitivity of pressure sensors by using as active component a hybrid architecture comprising a mille-feuille assembly of rGO separated by covalently tethered molecular linkers. In analogy with the Hooke's law, our results clearly demonstrate how the sensitivity is effectively improved when flexible molecular linkers are employed. In particular, the sensitivity of pressure sensor is significantly increased by functionalization of graphene with more flexible molecules. The pressure sensor based on graphene oxide chemically modified with triethylene glycol amine

(**rGO-R$_1$**) exhibits a sensitivity as high as 0.82 kPa$^{-1}$, short response time (24 ms), ultralow detection limit (7 Pa), high durability (over 2000 times) and flexibility. By taking advantage of the compatibility of graphene for on-the-skin applications, we have demonstrated how our hybrid multilayer architecture can be employed for health monitoring and can be easily transformed into a matrix, which allows a 3D mapping of the pressure exerted by different object thus providing also spatial information. The device additional features such low power consumption (0.2 V operating voltage), large-scale fabrication process, commercially available raw material and low cost, makes it an appealing candidate for the technological applications in wearable health monitoring device, multimotion detection robotic and internet of functions. Furthermore, our pressure sensor is fabricated by solution processing, thus it is compatible with printed electronics solutions.

## Experimental details

*Experimental details are available in the supporting information.*

## Supporting Information

Supporting Information is available from the Wiley Online Library or from the author.

## Acknowledgements

This work was supported by the European Commission through the Graphene Flagship Core 2 project (GA-785219), and the International Center for Frontier Research in Chemistry (icFRC), the Polish National Science Centre (Grant no. 2015/18/E/ST5/00188 and Grant no. 2016/23/N/ST5/00063). C.-B.H. acknowledges the Ernest Solvay Fund for a Ph.D. fellowship.

Received: ((will be filled in by the editorial staff))

Revised: ((will be filled in by the editorial staff))

Published online: ((will be filled in by the editorial staff))

References

[1] Y. P. Zang, F. J. Zhang, C. A. Di, D. B. Zhu, *Mater. Horizons* **2015**, *2*, 140.
[2] M. L. Hammock, A. Chortos, B. C. K. Tee, J. B. H. Tok, Z. N. Bao, *Adv. Mater.* **2013**, *25*, 5997.
[3] S. H. Wang, J. Xu, W. C. Wang, G. J. N. Wang, R. Rastak, F. Molina-Lopez, J. W. Chung, S. M. Niu, V. R. Feig, J. Lopez, T. Lei, S. K. Kwon, Y. Kim, A. M. Foudeh, A. Ehrlich, A. Gasperini, Y. Yun, B. Murmann, J. B. H. Tok, Z. A. Bao, *Nature* **2018**, *555*, 83.
[4] S. Jung, J. H. Kim, J. Kim, S. Choi, J. Lee, I. Park, T. Hyeon, D. H. Kim, *Adv. Mater.* **2014**, *26*, 4825.
[5] H. H. Chou, A. Nguyen, A. Chortos, J. W. F. To, C. Lu, J. G. Mei, T. Kurosawa, W. G. Bae, J. B. H. Tok, Z. N. Bao, *Nat. Commun.* **2015**, *6*, 8011.
[6] Z. Lou, S. Chen, L. L. Wang, K. Jiang, G. Z. Shen, *Nano Energy* **2016**, *23*, 7.
[7] Y. J. Gao, H. Ota, E. W. Schaler, K. Chen, A. Zhao, W. Gao, H. M. Fahad, Y. G. Leng, A. Z. Zheng, F. R. Xiong, C. C. Zhang, L. C. Tai, P. D. Zhao, R. S. Fearing, A. Javey, *Adv. Mater.* **2017**, *29*, 1701985.
[8] G. Schwartz, B. C. K. Tee, J. G. Mei, A. L. Appleton, D. H. Kim, H. L. Wang, Z. N. Bao, *Nat. Commun.* **2013**, *4*, 1859.
[9] E. Laukhina, R. Pfattner, L. R. Ferreras, S. Galli, M. Mas-Torrent, N. Masciocchi, V. Laukhin, C. Rovira, J. Veciana, *Adv Mater* **2010**, *22*, 977.
[10] L. Q. Tao, K. N. Zhang, H. Tian, Y. Liu, D. Y. Wang, Y. Q. Chen, Y. Yang, T. L. Ren, *Acs Nano* **2017**, *11*, 8790.
[11] M. M. Liu, X. Pu, C. Y. Jiang, T. Liu, X. Huang, L. B. Chen, C. H. Du, J. M. Sun, W. G. Hu, Z. L. Wang, *Adv. Mater.* **2017**, *29*, 1703700.
[12] X. W. Wang, Y. Gu, Z. P. Xiong, Z. Cui, T. Zhang, *Adv. Mater.* **2014**, *26*, 1336.
[13] H. B. Yao, J. Ge, C. F. Wang, X. Wang, W. Hu, Z. J. Zheng, Y. Ni, S. H. Yu, *Adv. Mater.* **2013**, *25*, 6692.
[14] Q. G. Wang, W. Hong, L. Dong, *Nanoscale* **2016**, *8*, 7663.
[15] D. H. Ho, Q. Sun, S. Y. Kim, J. T. Han, D. H. Kim, J. H. Cho, *Adv. Mater.* **2016**, *28*, 2601.
[16] S. Chun, H. Jung, Y. Choi, G. Bae, J. P. Kil, W. Park, *Carbon* **2015**, *94*, 982.
[17] D. J. Lipomi, M. Vosgueritchian, B. C. K. Tee, S. L. Hellstrom, J. A. Lee, C. H. Fox, Z. N. Bao, *Nat. Nanotechnol.* **2011**, *6*, 788.
[18] L. J. Pan, A. Chortos, G. H. Yu, Y. Q. Wang, S. Isaacson, R. Allen, Y. Shi, R. Dauskardt, Z. N. Bao, *Nat. Commun.* **2014**, *5*, 3002.
[19] R. R. He, P. D. Yang, *Nat. Nanotechnol.* **2006**, *1*, 42.
[20] Y. P. Zang, F. J. Zhang, D. Z. Huang, X. K. Gao, C. A. Di, D. B. Zhu, *Nat. Commun.* **2015**, *6*, 6269.
[21] M. Quintana, E. Vazquez, M. Prato, *Acc. Chem. Res* **2013**, *46*, 138.
[22] S. P. Pang, Y. Hernandez, X. L. Feng, K. Mullen, *Adv. Mater.* **2011**, *23*, 2779.
[23] S. P. Pang, J. M. Englert, H. N. Tsao, Y. Hernandez, A. Hirsch, X. L. Feng, K. Mullen, *Adv. Mater.* **2010**, *22*, 5374.
[24] L. Zhang, G. F. Hou, Z. Z. Wu, V. Shanov, *Nano Life* **2016**, *6*, 1642005.
[25] C. S. Boland, U. Khan, G. Ryan, S. Barwich, R. Charifou, A. Harvey, C. Backes, Z. Li, M. S. Ferreira, M. E. Mobius, R. J. Young, J. N. Coleman, *Science* **2016**, *354*, 1257.
[26] S. K. Ameri, R. Ho, H. W. Jang, L. Tao, Y. H. Wang, L. Wang, D. M. Schnyer, D. Akinwande, N. S. Lu, *Acs Nano* **2017**, *11*, 7634.

[27] L. H. Li, Y. Y. Bai, L. L. Li, S. Q. Wang, T. Zhang, *Adv. Mater.* **2017**, *29*, 1702517.
[28] S. Gong, W. Schwalb, Y. W. Wang, Y. Chen, Y. Tang, J. Si, B. Shirinzadeh, W. L. Cheng, *Nat. Commun.* **2014**, *5*, 3132.
[29] S. B. A. Liu, X. Wu, D. D. Zhang, C. W. Guo, P. Wang, W. D. Hu, X. M. Li, X. F. Zhou, H. J. Xu, C. Luo, J. Zhang, J. H. Chu, *ACS Appl. Mater. Interfaces* **2017**, *9*, 24148.
[30] X. D. Wang, M. L. Que, M. X. Chen, X. Han, X. Y. Li, C. F. Pan, Z. L. Wang, *Adv Mater* **2017**, *29*.
[31] C. L. Choong, M. B. Shim, B. S. Lee, S. Jeon, D. S. Ko, T. H. Kang, J. Bae, S. H. Lee, K. E. Byun, J. Im, Y. J. Jeong, C. E. Park, J. J. Park, U. I. Chung, *Adv Mater* **2014**, *26*, 3451.
[32] D. Kang, P. V. Pikhitsa, Y. W. Choi, C. Lee, S. S. Shin, L. F. Piao, B. Park, K. Y. Suh, T. I. Kim, M. Choi, *Nature* **2014**, *516*, 222.
[33] X. M. Li, T. T. Yang, Y. Yang, J. Zhu, L. Li, F. E. Alam, X. Li, K. L. Wang, H. Y. Cheng, C. T. Lin, Y. Fang, H. W. Zhu, *Adv. Funct. Mater.* **2016**, *26*, 1322.
[34] B. W. Zhu, Z. Q. Niu, H. Wang, W. R. Leow, H. Wang, Y. G. Li, L. Y. Zheng, J. Wei, F. W. Huo, X. D. Chen, *Small* **2014**, *10*, 3625.
[35] C. Pang, G. Y. Lee, T. I. Kim, S. M. Kim, H. N. Kim, S. H. Ahn, K. Y. Suh, *Nat. Mater.* **2012**, *11*, 795.
[36] H. Vandeparre, D. Watson, S. P. Lacour, *Appl. Phys. Lett.* **2013**, *103*.
[37] S. C. B. Mannsfeld, B. C. K. Tee, R. M. Stoltenberg, C. V. H. H. Chen, S. Barman, B. V. O. Muir, A. N. Sokolov, C. Reese, Z. N. Bao, *Nat. Mater.* **2010**, *9*, 859.
[38] X. Y. Zhang, A. Ciesielski, F. Richard, P. K. Chen, E. A. Prasetyanto, L. De Cola, P. Samori, *Small* **2016**, *12*, 1044.
[39] C. K. Chua, M. Pumera, *Chem Soc Rev* **2014**, *43*, 291.
[40] H. Lee, R. M. Venable, A. D. MacKerell, R. W. Pastor, *Biophys. J.* **2008**, *95*, 1590.
[41] R. Ramachandran, G. Beaucage, A. S. Kulkarni, D. McFaddin, J. Merrick-Mack, V. Galiatsatos, *Macromolecules* **2008**, *41*, 9802.
[42] G. Petekidis, D. Vlassopoulos, P. Galda, M. Rehahn, M. Ballauff, *Macromolecules* **1996**, *29*, 8948.
[43] H. Tian, Y. Shu, X. F. Wang, M. A. Mohammad, Z. Bie, Q. Y. Xie, C. Li, W. T. Mi, Y. Yang, T. L. Ren, *Sci. Rep.* **2015**, *5*, 8603.
[44] W. W. Nichols, *Am. J. Hypertens* **2005**, *18*, 3S.